Structural and Defect Study of $LiMn_2O_4$ Formation

V. Massarotti, M. Bini, and D. Capsoni

Department of Physical Chemistry of the University and CSTE-CNR, Viale Taramelli 16, I-27100 Pavia (Italy)

Z. Naturforsch. **51a**, 267–276 (1996); received March 3, 1996

The $LiMn_2O_4$ formation from MnO and Li_2CO_3 mixtures with lithium cationic fraction $0.31 \leq x \leq 0.40$ was studied by structural profile refinement from X-ray data, thermal (TGA and DSC) measurements and scanning electron microscopy (SEM) observations. Quantitative phase analysis, structural and microstructural parameters and composition of the coexisting phases were obtained.

Different behaviours were observed in the composition ranges $0.33 \leq x \leq 0.35$ and $x \geq 0.37$. In the former range only the stoichiometric spinel phase was obtained, in the latter, in addition to the Li_2MnO_3 compound, two spinel phases could be considered: I) $LiMn_2O_4$ stoichiometric spinel; II) $Li_{1+y}Mn_{2-y}O_4$ ($0.11 \leq y \leq 0.23$), a non-stoichiometric phase whose small particle size resulted practically independent of the initial composition and annealing temperature. Such a conclusion was supported also by SEM observations. The relative abundance of phase II increased with increasing lithium content and with decreasing temperature.

Key words: Solid state reaction, Lithium Manganese Spinel, Structural and microstructural parameters, Non-stoichiometry, Substitutional defects.

1. Introduction

Many transition metal oxides have peculiar physicochemical properties due to coupling of the cation electronic structure with the crystal field local value. Such compounds find applications as catalysts as well as electrolytes or electrode materials for electrochemical devices. In such a context a suitable way to assess the ternary oxides of the systems MeO-Li_2O (Me = V, Cr, Mn, Fe, Co, Ni) consists in preparing the pertinent compounds and characterizing the relationships occurring among composition, structure, microstructure and physical properties. Among the ternary compound families, the spinels are the most extensively studied ones, and the lithium manganese spinel, $LiMn_2O_4$, represents a very peculiar member of the family. For such a material, particularly for electrochemical applications, best stability against oxidation and high capability of lithium deintercalation are required [1]. It was previously shown that lithium can be removed from $LiMn_2O_4$ [2] and electrochemical reversible lithium intercalation is possible [3–5]. Moreover, the transformation $LiMn_2O_4 \rightleftarrows Li_2Mn_2O_4$ was later studied [6–9], and $LiMn_2O_4$ spinel as positive electrode for batteries was introduced [10–14]. The characterization of electrochemically optimized spinel samples is usually related to the nominal lithium content and the annealing conditions. However, more information is still needed about structural and microstructural parameters, non-stoichiometry and structural defects related to the actual composition and to the synthesis conditions of the samples.

The present paper was aimed at studying the formation of $LiMn_2O_4$ from the reactive system MnO/Li_2CO_3 and characterizing the structural and microstructural properties as functions of composition and annealing temperature. The structural parameters were determined by Rietveld profile refinement and the microstructural ones were obtained by both diffraction peak profile analysis and by SEM observations.

Reprint requests to Prof. V. Massarotti.

2. Experimental

2.1 Materials and Sample Preparation

The samples were prepared from Alfa (99.5%) MnO and Carlo Erba (R.P.) Li_2CO_3, the starting mixtures having the lithium cationic fraction, x, ranging between 0.31 and 0.40. Each mixture was fired in air for 8 h at 750 °C to obtain complete carbonate decomposition. Successive treatments for 8 h at 800 °C, 900 °C and 1000 °C and 1 h at 1100 °C were performed, and a sample was taken after each annealing step. Both heating and cooling rates were 5 °C/min. In some particular cases samples were prepared by rapid quenching from $800 \leq T \leq 1000$ °C.

0932-0784 / 96 / 0400-0267 $ 06.00 © – Verlag der Zeitschrift für Naturforschung, D-72072 Tübingen

2.2 Apparatus and Procedures

Diffraction data were obtained at room temperature by a Philips PW 1710 powder diffractometer equipped with a Philips PW 1050 vertical goniometer. Use was made of the CuKα radiation ($K\alpha_1 = 1.54056$ Å; $K\alpha_2 = 1.5443$ Å) obtained by means of a graphite monochromator. Patterns were collected in the angular range $15° < 2\theta < 130°$ in step scan mode (step width 0.02° and 0.025°; counting time 3 s and 10 s).

The thermal treatment of samples in the thermogravimetric cell was performed with a Stanton Redcroft TGA 762; for the DSC measurements use was made of a Stanton Redcroft DSC 1500, both connected to a Rheometrics Scientific Data Acquisition system. In both TGA and DSC analysis heating and cooling rates of 5 °C/min in air were used.

SEM micrographs were collected with a Cambridge Stereoscan 200 scanning electron microscope on gold sputtered samples (gold thickness about 100 Å).

Structural and profile parameters were obtained by the Rietveld refinement procedure [15]; the refinement was performed with the programs WYRIET version 3.5 [16] and DBWS 3.2 S [17]. A more detailed description about the Rietveld refinement of multiphase systems has been reported in a previous paper [18]. The structural model to fit the observed patterns depends on the mixture composition, which determines the presence and abundance of the following compounds:

i) $LiMn_2O_4$ – spinel type (Fd 3 m): cubic
$a \cong 8.2476$ Å

Li (8 a)	1/8, 1/8, 1/8	Tetrahedral site
Mn (16 d)	1/2, 1/2, 1/2	Octahedral site
O (32 e)	u, u, u	($u \cong 0.26$)

atomic positions deduced from [19]*;

ii) Mn_3O_4 – spinel type ($I4_1/amd$): tetragonal
$a \cong 5.7621$ Å, $c \cong 9.4696$ Å
atomic positions according to [20];

iii) Li_2MnO_3 (C 2/m): monoclinic
$a \cong 4.937$ Å, $b \cong 8.532$ Å, $c \cong 5.030$ Å, $\beta \cong 109.46°$
atomic positions according to [21].

At the beginning of the refinement procedure, scale factors, background coefficients and lattice parameters (initial values starting from those obtained in a least squares fit) were varied. The profile coefficients of a Pearson VII or pseudo-Voigt function were refined. Finally, structural parameters, atomic coordinates for spinel oxygen, occupancy and isotropic thermal factors, were refined. The spinel stoichiometry was estimated assuming the tetrahedral site totally occupied by Li. The occupancy of Mn ion on the octahedral site was refined: when a value appreciably lower than unity was obtained, also the Li occupancy on the site was considered and the sum of the occupancies contrained to unity.

* According to the computer program requirements, fractional coordinates with respect to the origin at the centre were used.

3. Results and Discussion

3.1 Phases Coexistence and Lattice Parameter

The presence of single phase $LiMn_2O_4$ was observed for $0.33 \leq x \leq 0.35$, while the structural profile refinement could be favourably performed on X-ray data from the pertinent samples obtained at any temperature. Figure 1 shows the comparison between the observed ($x = 0.33$ sample annealed at 800 °C) and calculated profile after refinement. The spinel phase was nearly stoichiometric within the experimental errors. Tetragonal Mn_3O_4 (and also Mn_2O_3 traces at lower temperatures) in addition to the spinel phase, is also present for $x \leq 0.33$, and monoclinic Li_2MnO_3 for $x > 0.35$. Concerning the extreme compositions on the lithium-rich side (to which this paper is mainly devoted) the following remarks can be made.

i) The difficulty of Rietveld profile analysis increases when x departs from the monophasic range. However, that should not be due to the presence of a few percent of a second phase, whose structural features might be taken into account quite accurately in a complete structural model.

ii) The value of the spinel lattice parameter is strongly dependent on the lithium content of the starting mixture. Figure 2 a reports the lattice parameter as a function of temperature for each x. Appreciable variation of a is indeed found also between the $x = 0.33$ and $x = 0.35$ samples, although the spinel phase composition results unchanged. It can be considered that the precision of cation occupancy factors, obtained from structural refinement, is insufficient to relate the a parameter to a possible variation of defects. Perhaps, a very low fraction of a substitutional defect (inverted cations) may have a sensible effect on the lattice parameter.

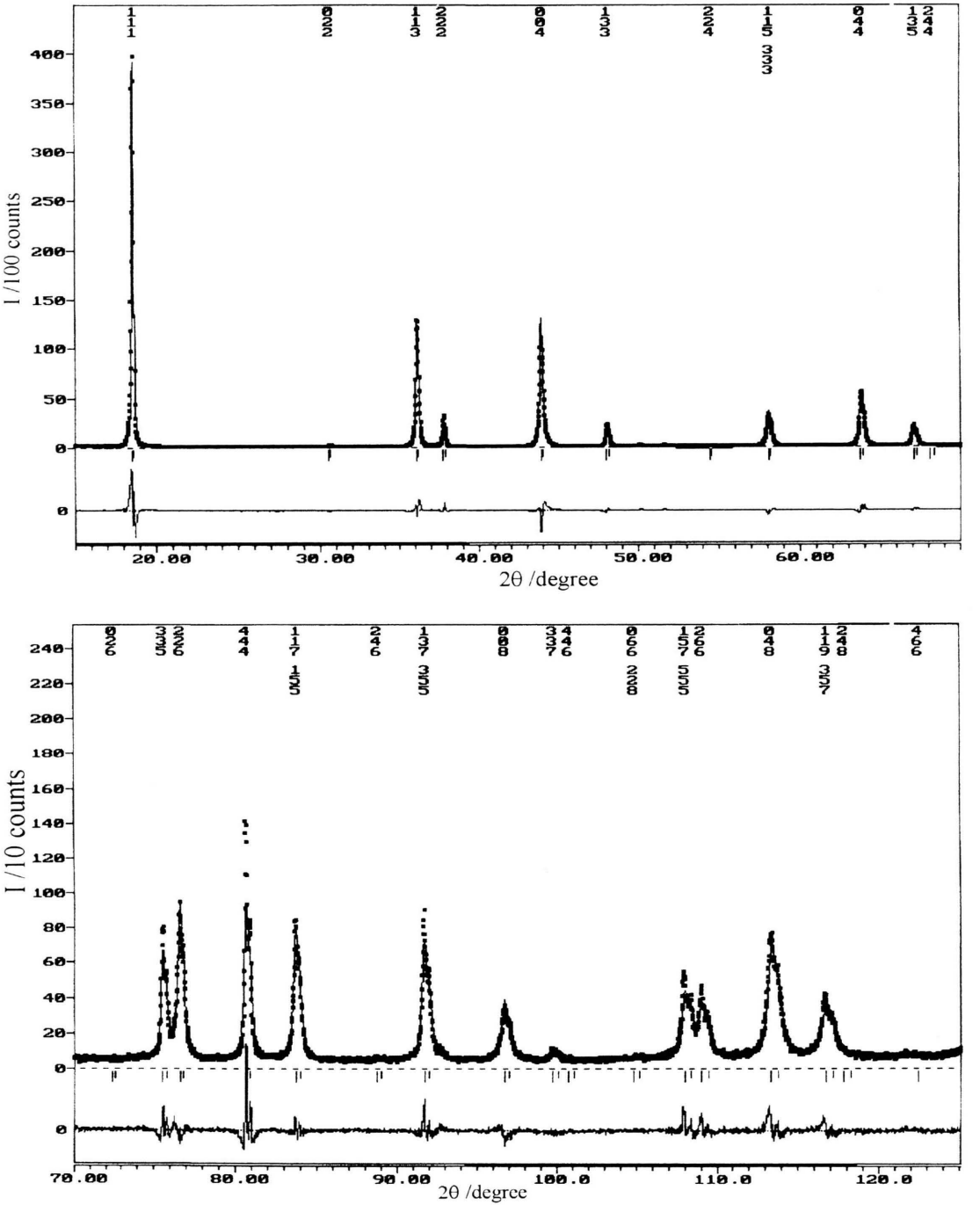

Fig. 1. Comparison between observed (dots) and calculated (solid line) X-ray profile after refinement for the $x = 0.33$ sample annealed at 800 °C. In the lower part the difference is plotted, in the upper part the hkl reflection indices are reported.

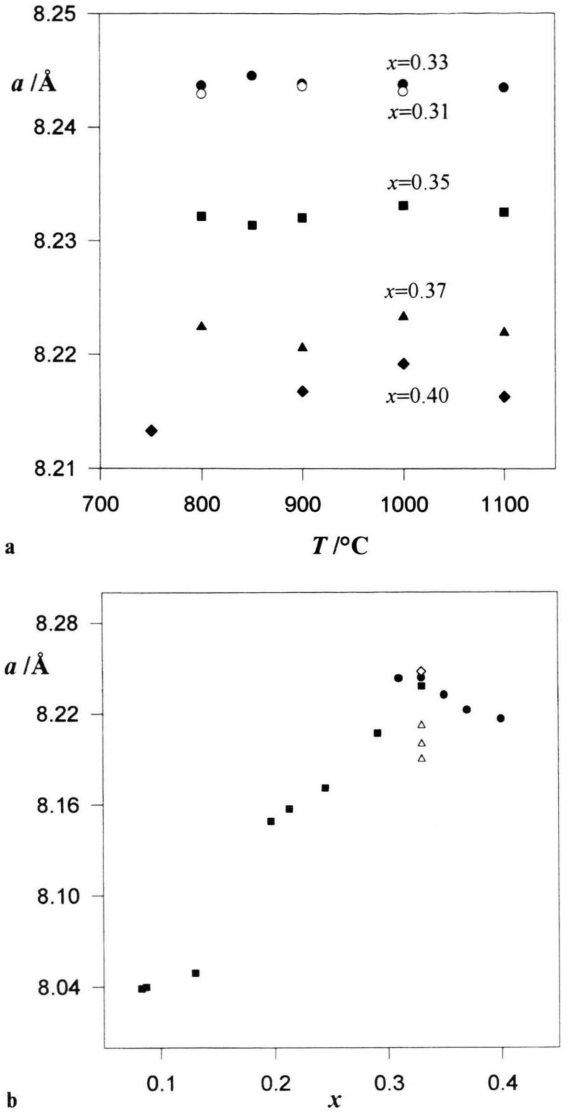

Fig. 2. (a) Annealing temperature dependence of the spinel lattice parameter for samples $x = 0.31$ (○), 0.33 (●), 0.35 (■), 0.37 (▲) and 0.40 (◆); (b) x dependence of mean values a (●) and comparison with literature data: (△), [8]; (■), [5] and (◇), [19].

iii) The annealing temperature has no influence on the lattice parameter, as can be seen from the trend of the values reported in Figure 2a. No discontinuity is observed near 950 °C, where a $LiMn_2O_4$ decomposition reaction takes place [19]. In Fig. 2b the a values, averaged over different temperatures (closed circles), are reported as function of x and compared with literature data in the range $8.190 < a/Å < 8.247$ obtained by several authors for the stoichiometric spinel after different synthesis conditions [5, 8, 19]. Those pertinent to samples obtained by delithiation [5] (for $x < 0.30$) show a wide range of lattice parameter values (8.040–8.207 Å).

3.2 DSC and TGA Measurements

To investigate the nature and reversibility of the spinel decomposition process, DSC and TGA measurements were performed on $x = 0.35$ samples annealed at 800 °C. The DSC results gave an endothermal change of enthalpy (170 J/g) on heating with a sharp peak starting at 939 °C, reaching a maximum at 946 °C, then slowly returning to the baseline at 1000 °C. An exothermal comparable change was observed on cooling, although with a broader peak, starting at 990 °C, reaching a maximum at 880 °C and returning to the baseline at 865 °C. A significant change in the peak shape and appreciable hysteresis were observed in the present experimental conditions.

The TGA results showed a slight weight increase from room temperature up to 690 °C (+ 0.4%), that might correspond to the initial presence of a slight oxygen deficiency, according to the formula $LiMn_2O_{3.952(15)}$, not revealed in the structural determination on the 800 °C annealed sample. Then, other distinct changes could be observed:

- a slow weight loss up to 790 °C (−0.2%), where an increase of the loss rate is observed;
- a higher increase of the loss rate at 963 °C (−1.32%), above which temperature the weight loss continued monotonically up to 1100 °C (−5.10%), where the change was not completely over.

During cooling down to 620 °C the same total weight change was observed. The non-monotonic increase showed rate changes at 1090, 920 and 897 °C, below which a linear trend was maintained down to 620 °C. It can be deduced that, under the same experimental conditions as for DSC experiments, a nearly complete reversibility of the process is obtained. However, a sensible hysteresis was revealed by the TGA plots too, more evident when higher cooling rates were used. The observed mass changes fairly agree with the expected value (5.89%) for the complete reversible process

$$3\,LiMn_2O_4 \rightleftarrows Mn_3O_4 + 3\,LiMnO_2 + O_2\,,$$

according to which the degree of transformation achieved at 1100 °C was about 0.87. On the other hand, rapid quenched samples can preserve Mn_3O_4 and $LiMnO_2$ phases at room temperature.

On comparing DSC and TGA data, it can be deduced that the endothermal enthalpy change is complete ($939 \leq T \leq 1000$ °C) when the degree of transformation varies from 0.18 to 0.55. Moreover, on cooling, the enthalpy change is complete ($990 \geq T \leq 865$ °C) when the degree of transformation goes back from 0.58 to 0.10, i.e., the enthalpy change occurs in a temperature range much more limited than that required for the weight change. Both endothermal and exothermal processes are always related to the highest weight change rate, and the energy exchange is faster than release or gain of oxygen at the surface of the solid phases in the temperature range and at the oxygen partial pressure of the process, possibly due to diffusion phenomena through the solid.

3.3 Peak Profile Analysis and Profile Refinement Model

It is well known that the profile refinement of the diffraction patterns can give indications about the influence of the initial bulk composition both on the abundance of phases and on the cations content of each phase. However, to perform an accurate structural refinement by pattern fitting, the most reliable crystal model and best profile peak shape are required. The most accurate profile investigation has been performed on the hhh peaks series, for which splitting should be evident in odd terms in cases of tetragonal distortion, like that described by the $I4_1/amd$ space group [22]. Such a crystal modification, proposed for chemically lithiated $Li_{1+\delta}Mn_2O_4$ samples, can be ruled out for our Li-rich samples ($x \geq 0.35$) after complete profile analysis. Really both even and odd index peaks of a given pattern have substantially the same shape and a well defined angular dependent broadening. On the contrary, samples of different composition can have a quite different profile shape and broadening. As an example of different profile shapes we show in Fig. 3 the comparison of the 444 diffraction peak for the $x = 0.33$ and $x = 0.37$ samples, annealed at 800 °C. The angular shift towards higher angles for the $x = 0.37$ sample is due to the lower a value. Moreover, higher intensity than expected near the $K\alpha_2$ angular position makes it necessary to consider another diffraction component not present in the $x = 0.33$ (and $x = 0.35$) sample. In other words, a higher asymmetry of the peak is observed because of the presence of an additional diffraction component. Asymmetry would become more evident if $K\alpha_2$ radiation stripping were applied on the diffraction data of both peaks. Another difference can be noted between the two 444 peak profiles: the $x = 0.33$ peak can easily be fitted by one p-Voigt function (see Fig. 4a) while that of $x = 0.37$ cannot. In the latter case a comparable result can only be obtained by using two p-V functions (see Figure 4b). The fitting function at lower angles (I) results practically gaussian (G), while the feature of the higher angle function (II) is nearly lorentzian (L). The integral breadth of the L component is very large in comparison with that of the G one. It can be observed that the impossibility of describing the diffraction profile by means of a single function makes it possible to predict worse results in the profile refinement using a model of one cubic spinel phase, and the additional monoclinic Li_2MnO_3 phase. Such a model gives both unsatisfactory peak profile refinement and unreliable mean values of the lattice parameter. In addition, the use of a single spinel phase refinement would give an overestimate of the Li_2MnO_3 percentage in comparison with the expected values. Indeed, according to the extrapolation from the calculated by one pseudo-Voigt function $x = 0.4$ (18.3(1.5)%) and the $x = 0.37$ (13.0(1.2)%) values, about 9 and 6% of Li_2MnO_3 should be present in $x = 0.35$ and in $x = 0.33$ samples respectively. Such a conclusion, however, disagrees with the experimental evidence (see § 3.1).

3.4 Structural Refinement by a Two-Phases Spinel Model

As previously noted, the shape of the diffraction profiles becomes more and more complex with increasing lithium content above $x = 0.37$. Owing to the presence of additional diffraction effects, very close to the cubic reflections and not due to tetragonal distortion, the use of two independent profiles in the fit procedure, accounting for two cubic spinel phases slightly different in composition and lattice parameter, may seem a satisfactory approximation. The first question that might arise refers to the evident and systematic change of the two p-V profiles: I tends towards the gaussian limit and II towards the lorentzian one. If one can think about the coexistence of two limiting spinel phases represented by two series of peaks I and II, then one must look for the meaning

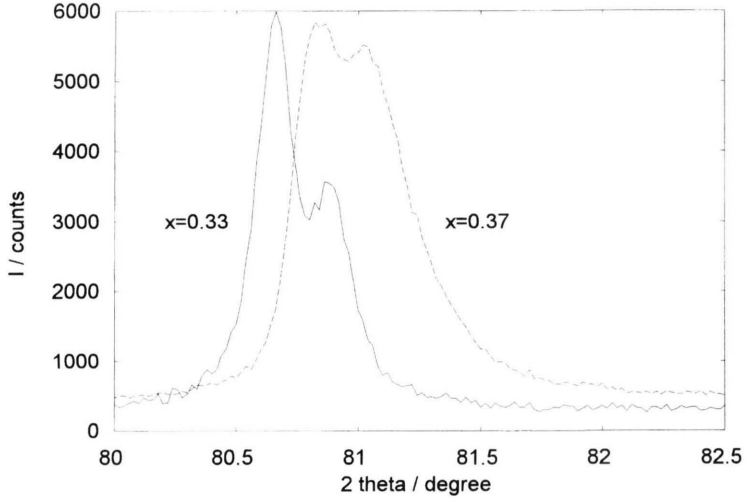

Fig. 3. Comparison of the diffraction profiles of 444 reflection for $x = 0.33$ and $x = 0.37$ samples.

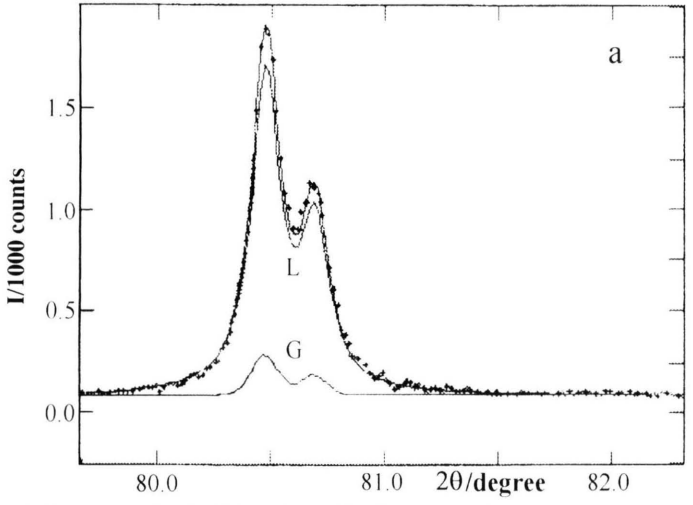

Fig. 4. Pseudo-Voigt (solid line) profile fit of the observed data (+): a) 1 p-Voigt function ($x = 0.33$); b) 2 p-Voigt functions ($x = 0.37$). The gaussian (G) and lorentzian (L) components are plotted (see text).

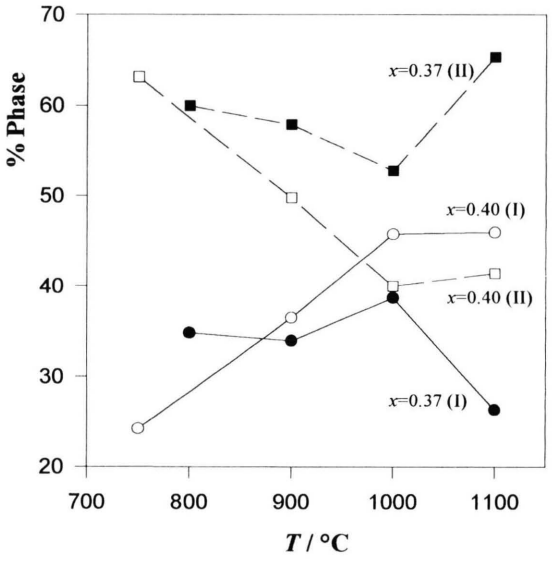

Fig. 5. Temperature dependence of the percentage abundance of spinel I and II phases for the $x = 0.37$ and $x = 0.40$ samples. The mean percentage values for the monoclinic Li_2MnO_3 phase are 7.8(0.8)% and 13,4(1.4)% respectively.

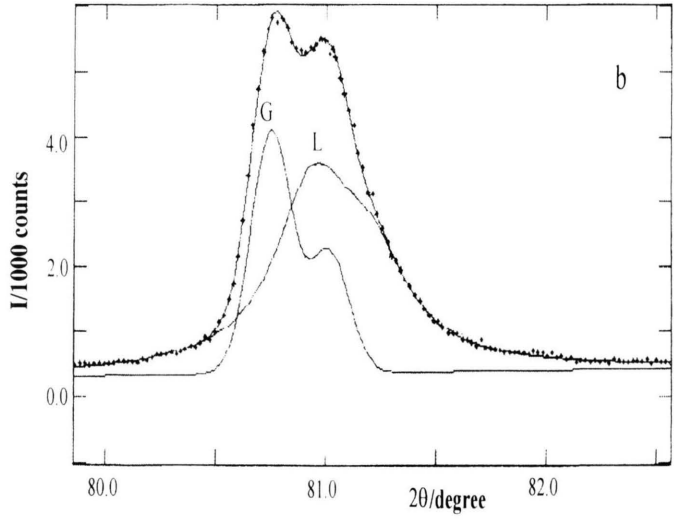

of their limiting shapes, G and L, respectively. In other words, the first, lower angle peak set has a sharp gaussian shape with practically strain contribution only. On the contrary, the second, higher angle peak set has a broad lorentzian shape, mainly representing the size contribution of the pertinent phase. It can be observed (Fig. 4 b) that the maximum of the G function is always very close to the angular position of the intensity maximum of the complex diffraction peak, while the L function has its maximum close to the $K\alpha_2$ position. If one considers the G-component set as the diffraction effect of the stoichiometric spinel phase, and the L-component set as the diffraction effect of a non stoichiometric phase or range of non stoichiometric spinel phases, one can also understand the possible influence of the composition range breadth on peak broadening, and hence on the crystallite size determination. Therefore, the complete model for the refinement must take into account three phases: two cubic spinels and the monoclinic Li_2MnO_3.

The reliability of the hypothesis concerning the stoichiometric composition of the "Spinel I" phase has been tested and ascertained in several cases. The exclusive occupancy of the tetrahedral site by lithium atoms can be inferred from the very low observed intensity of 22 *l* reflections, strongly dependent on the atomic scattering factors of the ions in the (8 a) positions. On the other hand, the exclusive presence of Mn atoms on the (16 d) octahedral sites has been verified by refining the occupancy factor. Subsequently, the cationic occupancy factors have been fixed to unity to gain stability during the three-phase refinement. The discrepancy factors of these refinements are much better than those obtained by the two-phase model. In Table 1 the comparison between the results of the two models for the $x = 0.37$ sample, annealed at 800 °C, are reported.

Table 1. Comparison between the refinement results obtained by the two-phase and the three-phase model for the $x = 0.37$ sample annealed at 800 °C.

	Two-phase model (one spinel phase)	Three-phase model (two spinel phases)
Stoichiometric spinel		
R_B [a]	4.23	4.78
% Phase	88.40	34.81
a/Å	8.2224 (1)	8.2287 (1)
u [b]	0.2642 (2)	0.2638 (1)
Formula	$Li_{1.06(2)}Mn_{1.94(2)}O_4$	$LiMn_2O_4$
Non stoichiometric spinel		
R_B [a]		2.91
% Phase		58.58
a/Å		8.2028 (2)
u [b]		0.2638 (1)
Formula		$Li_{1.19(2)}Mn_{1.81(2)}O_4$
Monoclinic Li_2MnO_3		
R_B [a]	14.27	13.69
% Phase	11.60	6.61
a/Å	4.8989 (5)	4.9221 (2)
b/Å	8.5452 (10)	8.5276 (4)
c/Å	5.0211 (5)	5.0395 (3)
β/°	108.663 (7)	109.368 (4)
Global parameters & factors		
R_p [c]	10.10	7.40
R_{wp} [d]	14.10	10.53
S [e]	2.81	2.10
x_t [f]	0.39	0.39

[a] Bragg discrepancy factor
[b] Oxygen coordinate
[c] Profile discrepancy factor
[d] Weighted profile discrepancy factor
[e] Goodness of fit
[f] Total lithium cationic fraction of the sample, calculated from abundance and Li content of each phase.
The meaning of the above discrepancy factors is reported in [17].

The observed temperature dependences of the percentage abundance of spinel I and II phases for the $x = 0.37$ and $x = 0.40$ samples are reported in Figure 5. For the $x = 0.37$ samples, it can be seen that the quantities of the two spinel phases have substantially reached definitive values after the first treatment at 800 °C although more appreciable deviations (slightly large than the experimental error) can be observed after the 1000 °C and 1100 °C annealings. On the other hand the $x = 0.40$ samples show larger variations for phases I and II percentages for increasing temperatures. Phase II is prevalent at 750 °C, then it converts partially into stoichiometric phase I, while the lithium content slightly increases in the residual phase II, whose composition changes from $(Li_{1.18(2)}Mn_{1.82(2)}O_4)$ at 750 °C to $(Li_{1.23(2)}Mn_{1.77(2)}O_4)$ at 1100 °C. The total lithium content, taking into account the contribution of all phases present in the samples, ranges between 0.395 and 0.411.

In the composition range $0.37 \leq x \leq 0.40$, the difference between the a values obtained for the two spinel phases results quite independent of both x and the annealing temperature.

3.5 Microstructural Determination

3.5.1 Peak Broadening Analysis

The peak integral breadths were determined both for spinel samples and BaF_2 as a standard [23], using

the p-V function. After correction for instrumental effects, the sample broadening components (gaussian β_G^f and lorentzian β_L^f) were obtained and the contribution of both size and strain effects were ascertained by the Hall and Williamson plot [24]. The mean crystallite size, D, and the micro-strain parameter $e = \Delta d/d$ (where d represents the interplanar distance of the planes family) were deduced by the Langford method [23] according to the formulas

$$\langle D \rangle = \frac{\lambda}{\beta_L^f \cos \vartheta}, \quad e = \frac{\beta_G^f}{4 \tan \vartheta}.$$

The analysis of profile reflections belonging to the same family hhh was also performed on the basis of the Warren-Averbach method [25, 26]. The average crystallite size and microstrain values obtained by the latter method agree with the pertinent values deduced by the former approach. Figure 6 shows the trend of the D values as functions of the annealing temperature, for each x. D increases with the annealing temperature and the increasing rate reaches its maximum for $x = 0.35$. Very small crystallite sizes, nearly independent of temperature, were observed when two cubic spinel phases are present. In this case the crystallite size was determined from the spinel II phase contribution, and pertinent values are reported in Fig. 6 for $x = 0.37$ and $x = 0.40$ samples.

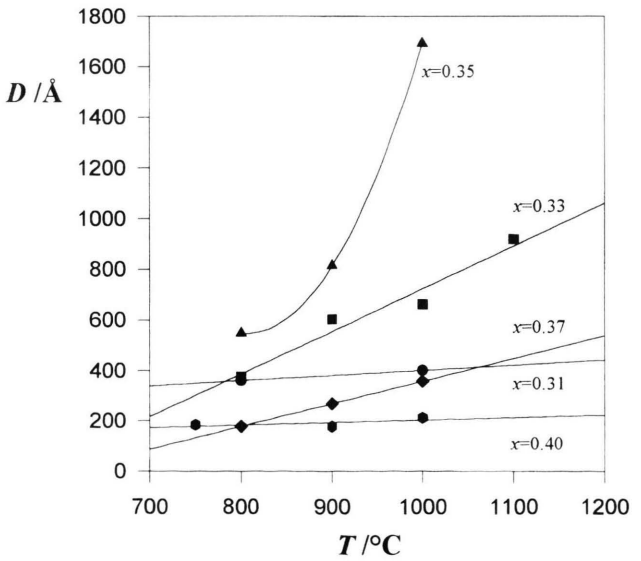

Fig. 6. Mean crystallite diameter D as a function of the annealing temperature, for each composition set of the samples. The data for the $x = 0.37$ and $x = 0.40$ samples are pertinent to the phase II spinel component.

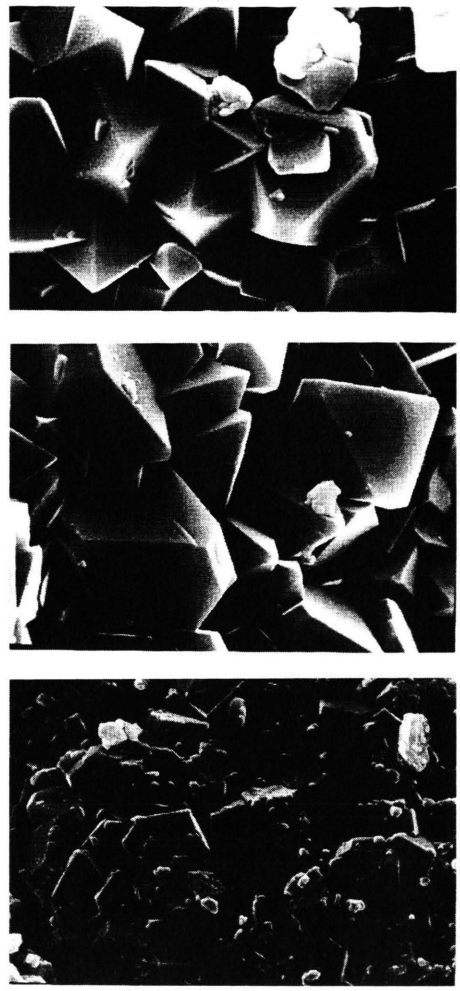

Fig. 7. SEM micrographs of the samples annealed 8 h at 1000 °C (a) $x = 0.33$, 10 kX; (b) $x = 0.35$, 6.68 kX and (c) $x = 0.37$, 5.61 kX.

For what concerns the microstrain parameter e, a linear dependence of $\log e$ on x, independent of the annealing temperature, was found for $0.31 \leq x \leq 0.37$:

$$\log e = 20.8357\, x - 10.5343, \quad R = 0.983,$$

while a nearly constant value $e = 1.3 \cdot 10^{-3}$ was found for $x \geq 0.37$.

3.5.2 SEM Observations

Further evidence of the spinel phase formation as a function of composition is given by comparison of SEM micrographs taken on different samples subjected to the same annealing procedure. The morphology of Fig. 7 (a, b and c) shows the large increase of the

particle size when the lithium content increases from $x = 0.33$ to $x = 0.35$. A further increase to $x = 0.37$ produces smaller particles and two kinds of morphologies. The octahedral forms, the only present for $0.33 \leq x \leq 0.35$, are typical of the spinel phase. For higher x values, other smaller particles, round in shape and with very different electron scattering behaviour are formed. Such a trend is peculiar of the above composition range, independent of the annealing temperature, and the particle size is in good agreement with the crystallite size determined by the peak broadening analysis.

4. Conclusions

The present results put into evidence two different behaviours in the two composition ranges $0.33 \leq x \leq 0.35$ and $x \geq 0.37$. In the first case, only a stoichiometric spinel phase is formed whose lattice parameter depends on x, while the crystallite size depends both on x and temperature and the strain effects depend only on composition. On the contrary, from Li-rich samples two distinct spinel phases are formed:

I) $LiMn_2O_4$, stoichiometric. It contributes very sharp peaks to the powder diffraction profile, and its most evident features are strain effects, independent both of composition and annealing temperature.

II) $Li_{1+y}Mn_{2-y}O_4$, non stoichiometric. The diffraction peaks are very broad, due to the small particle size, and practically independent of composition and annealing temperature. Whether a real composition range may exist, contributing to the lorentzian peak broadening, still remains an open question. Moreover, the mean phase composition corresponds to an evident Li excess, constituting the substitutional defect Li_{Mn} on the spinel octahedral site. According to the configuration $[Li_1]_{8a}[Li_y Mn^{3+}_{1-3y} Mn^{4+}_{1+2y}]_{16d}O_4$, the mean oxidation state of Mn ion, $\langle V(Mn)\rangle = (7\text{-}y)/(2\text{-}y)$ can be determined. The highest observed value 3.83 is obtained for $y = 0.23$ pertinent to the $x = 0.40$ sample. The same kind of defect, although not revealed by the refinement procedure, might be present at a much lower concentration is samples having the lithium cationic fraction in the range 0.33–0.35, where a single spinel phase is observed with the lattice parameter depending on composition. A non-stoichiometric spinel phase, synthesized by chemical lithiation of $LiMn_2O_4$, was previously reported [2, 3, 5, 22, 27] as example of an interstitial (16c sites) compound, whose possible configurations are consistent with a corresponding reduction of Mn^{4+} to Mn^{3+}. In this case a structure distorsion at room temperature was observed, due to a cooperative Jahn-Teller effect.

On the basis of the present results, the need for further information can be inferred. As previously reported, composition, relative abundance and microstructural features of the phase depend on the initial composition and annealing temperature. It can be understood that the possibility exists for easy correlations between those data and other physical properties, such as electronic and/or ionic conductivity, magnetic susceptivity, and EPR signal and relaxation time in ^7Li NMR experiment, to gain completeness in materials characterization. Moreover, the same methodology may be useful in a large series of mixed oxides, particularly when a transition cation having different possible oxidation states is concerned.

Acknowledgement

This work has been supported by MURST 40% funds.

[1] J. M. Tarascon, W. R. McKinnon, F. Coowar, T. N. Bowmer, G. Amatucci, and D. Guyomard, J. Electrochem. Soc. **141,** 1421 (1994).
[2] J. C. Hunter, J. Solid State Chem. **39,** 142 (1981).
[3] M. M. Thackeray, W. I. F. David, P. G. Bruce, and J. B. Goodenough, Mat. Res. Bull. **18,** 461 (1983).
[4] J. B. Goodenough, M. M.Thackeray, W. I. F. David, and P. G. Bruce, Rev. Chim. Miner. **21,** 435 (1984).
[5] M. M. Thackeray, P. J. Johnson, L. A. de Picciotto, P. G. Bruce, and J. B. Goodenough, Mat. Res. Bull. **19,** 179 (1984).
[6] T. Nagaura, M. Yokokawa, and T. Hashimoto, U. K. Pat. Appl. 2, 196, 875 (1988).
[7] T. Nagaura, M. Yokokawa, and T. Hashimoto, U. S. Pat. Appl. 4, 828, 834 (1989).
[8] G. Pistoia, G. Wang, and C. Wang, Solid State Ionics **58,** 285 (1992).
[9] M. M. Thackeray, A. de Kock, M. H. Rossouw, D. Liles, R. Bittihn, and D. Hoge, J. Electrochem. Soc. **139,** 363 (1992).
[10] J. M. Tarascon and D. Guyomard, J. Electrochem. Soc. **138,** 2864 (1991).
[11] D. Guyomard and J. M. Tarascon, J. Electrochem. Soc. **139,** 937 (1992).
[12] D. Guyomard and J. M. Tarascon, High Power Ambient Temperature Lithium Batteries, W. D. K. Clark and G.

Halpert, Editors, PV 92-15, p. 113, The Electrochemical Society Proceedings Series, Pennington, NJ, 1992.
[13] J. M. Tarascon and D. Guyomard, Electrochim. Acta **38,** 1221 (1993).
[14] J. M. Tarascon, D. Guyomard, and G. L. Baker, J. Power Sources **43–44,** 689 (1993).
[15] H. M. Rietveld, J. Appl. Cryst. **2,** 65 (1969).
[16] J. Schneider, Proceeding IUCR Int. Workshop on the Rietveld Method, Petten 1989.
[17] D. B. Wiles and R. A. Young, J. Appl. Cryst. **14,** 149 (1981).
[18] V. Massarotti, D. Capsoni, and M. Bini, Z. Naturforsch. **50a,** 155 (1995).
[19] D. G. Wickham and W. J. Croft, J. Phys. Chem. Solids **7,** 351 (1958).
[20] K. Satomi, J. Phys. Soc. Japan **16,** 258 (1961).
[21] P. Strobel and B. Lambert-Andron, J. Sol. State Chem. **75,** 90 (1988).
[22] W. I. F. David, M. M. Thackeray, L. A. de Picciotto, and J. B. Goodenough, J. Solid State Chem. **67,** 316 (1987).
[23] J. I. Langford, NIST (Gaithersburg, MD), Spec. Pub. **846,** 110 (1992).
[24] W. H. Hall and G. K. Williamson, Proc. Phys. Soc. **64B,** 937 (1951).
[25] B. E. Warren and B. L. Averbach, J. Appl. Phys. **21,** 595 (1950).
[26] B. E. Warren, X-ray diffraction, Addison-Wesley Publishing Company, London 1969, Chapters 12–13.
[27] A. Mosbah, A. Verbaere, and M. Tournoux, Mat. Res. Bull. **18,** 1375 (1983).